Influence of Crystallization Conditions on Crystal Morphology and Size of $CaCO_3$ and Their Effect on Pressure Filtration

Ralf Beck and Jens-Petter Andreassen
Dept. of Chemical Engineering, Norwegian University of Science and Technology (NTNU), Trondheim 7491, Norway

DOI 10.1002/aic.12566
Published online March 7, 2011 in Wiley Online Library (wileyonlinelibrary.com).

The temperature, supersaturation, seeding procedure, stirring speed and other parameters were varied in crystallization experiments of calcium carbonate performed in aqueous solutions to control size, particle size distribution and morphology of the particles. Particle size information was obtained by focused beam reflectance measurements and the Coulter Counter Multisizer. Crystals of $CaCO_3$ could be crystallized as spherical polycrystalline particles of the vaterite polymorph, needle-like crystals of aragonite and both cube-like and novel plate-like crystals of calcite. Filtration experiments for calcium carbonate, performed at a constant pressure difference of 2 bar, show that spherical particles with a larger size show better filterability and that spheres with a wider size distribution, as a result of high supersaturation and nucleation, give higher average cake resistance values. Comparing different particle morphologies, plate-like crystals and needle-like crystals show worse filterability than spherical particles and cube-like particles. © 2011 American Institute of Chemical Engineers *AIChE J,* 58: 107–121, 2012
Keywords: calcium carbonate, crystallization (precipitation), focuses beam reflectance measurement (FBRM), solid/liquid separations, constant pressure cake filtration

Introduction

The performance of the solid-liquid separation stage depends strongly on crystal properties like size and shape which are determined by the environment of the preceding crystallization process.[1] Solid-liquid separation involves the separation of a solid and a liquid phase from a suspension. Sedimentation, centrifugation and centrifugal sedimentation (used in hydrocyclones) are examples for methods allowing for the separation of solids from a liquid phase.[2] In many industrial processes filters are used to fulfil this separation task. Among these are processes which apply the cake filtration-, depth filtration- and cross flow filtration principle. The scope of this article only comprises cake filtration (at constant pressure) and in the following only this separation technique is therefore considered.

The most widely applied relationship between permeability, size, and bed porosity stems from the work of Carman[3–5] which is found on Kozeny's considerations. In his work on liquid flow through a packed bed of solids Kozeny[6] regards the pore spaces within the particle bed as being equal to a bundle of parallel capillaries with a common equivalent diameter. By utilizing the well-known Poiseuille's law for laminar fluid flow in capillary tubes, Carman established a relation between bed porosity, specific surface and permeability. The following equation for the specific cake resistance, α_v, (in m^{-2}) is derived from the considerations of Carman and Kozeny[7]:

Correspondence concerning this article should be addressed to R. Beck at RalfB@chemeng.ntnu.no.

$$\alpha_V = 36\,C\,\frac{(1-\varepsilon)^2}{\varepsilon^3}\,\frac{1}{D_{32}^2} \tag{1}$$

In this equation ε is the particle bed porosity and D_{32} is the surface to volume mean size of (monosized) spheres, also called Sauter mean diameter. The particle bed porosity is defined by the ratio of the voids volume V_v and the total volume V_{tot} of the cake:

$$\varepsilon = \frac{V_v}{V_{tot}} \tag{2}$$

The relation between the Sauter mean diameter and the specific surface area

$$S_V = \frac{A_s}{V_s} \tag{3}$$

(A_s is the particles' surface area and V_s is the volume of the particles) is given by the following equation:

$$D_{32} = 6\,\frac{1}{S_V} \tag{4}$$

From Eq. 1 it can be seen that smaller particles (smaller D_{32}) with a higher specific surface area give rise to higher cake resistance values and therefore to worse filtration behavior. The Carman-Kozeny constant, C, depends on the tortuosity which accounts for the actual fluid path length through the bed, and the shape of the cross-section of a channel through which fluid is passing.[8] Assuming the average flow to be in a direction of 45° to the inflow surface of the bed, and either rectangular, annular or elliptical shapes of the capillaries, K equals to a value of 5 (Ref. 8). Experimental tests for spherical, incompressible particles have verified a value of ~5 for the Carman-Kozeny constant.[9]

In practice, however, suspensions are often composed of nonspherical particles exhibiting a variation in size. This has lead to concepts that are based on the Sauter mean diameter being calculated from the whole particle size distribution, and shape factors correcting for the deviation from spherical shapes.[10,11] In case of nonspherical particles Eq. 1 can be written as

$$\alpha_v = 36\,C\,\frac{(1-\varepsilon)^2}{\varepsilon^3}\,\frac{1}{D_{sv}^2} \tag{5}$$

where D_{sv} is the surface to volume mean size of particles of any shape. Defining a shape factor, ψ, for example as follows in terms of D_{sv} and the Sauter mean diameter D_{32}[11]:

$$\Psi = \frac{D_{sv}}{D_{32}} \tag{6}$$

Equation 5 can be rewritten as:

$$\alpha_V = 36\,\frac{C}{\Psi^2}\,\frac{(1-\varepsilon)^2}{\varepsilon^3}\,\frac{1}{D_{32}^2} \tag{7}$$

The shape factor, Ψ, is 1 for spheres and smaller than 1 for particles with a shape deviating from spheres. For a comprehensive account of other relationships between cake resistance (and permeability) and particle characteristics, reference should be made to Ref. 12. This reference includes the model of Hagen-Poiseuille, Richardson-Zaki, and Happel-Brenner.

For constant pressure filtration experiments the general filtration equation[10] which derives from d'Arcys equation[13] applied both to the filter medium and the filter cake, can be written in the following form:

$$\frac{t}{V} = \alpha_m\,\frac{\eta\,c_s}{2\,A^2\Delta p}\,V + \frac{\eta\,\beta}{A\,\Delta p} \tag{8}$$

where t is time, V is the filtrate volume, α_m is the average specific cake resistance in (m/kg), η is the dynamic viscosity of the liquid phase, c_s is the effective solids concentration in kg dry cake/m^3 filtrate,[10] A is the filter area, Δp is the applied pressure difference and β is the filter medium resistance. From this equation the specific cake resistance can be calculated based on experimental data allowing for the comparison of suspension filterability. There are several assumptions under which Eq. 8 has been derived. First, the feed suspension concentration is assumed to be constant and sedimentation does not occur. Then, liquid (with Newtonian rheology) is flowing through the incompressible cake in a laminar way. A direct consequence of these assumptions is that the cake height increases proportionally to the filtrate volume obtained per unit time. Finally all particles are assumed to deposit either on the surface of the filter cloth or on the topmost layer of the developing filter cake implying that particles do not enter the filtrate stream. The relationship between the specific cake resistance in m/kg (α_m) and in m^{-2} (α_v) is given by the following equation[7]:

$$\alpha_m = \alpha_V\,\frac{1}{\rho_s(1-\varepsilon)} \tag{9}$$

where ρ_s is the solid's density and ε is the porosity.

This work is part of an industrially sponsored project. Polycrystalline particles with a roughly spherical shape were identified in the industrial production of a secondary aromatic amine derivative, where filtrations problems are considered to be the major bottle neck. The striking similarity to polycrystalline particles L-glutamic acid motivated a comparative study of both these organic substances with respect to crystallization from aqueous solutions[14] and their filtration behavior.[15] To fulfil this task in a broader context a third, inorganic substance had to be selected which could be precipitated as polycrystalline spheres. Calcium carbonate was chosen as an inorganic counterpart crystallizing as particles exhibiting polycrystalline features[16] because of its importance in oil and gas industry where both precipitation phenomena and solid-liquid separation are crucial for efficient solid liquid-separation. The importance of calcium carbonate furthermore resides in its wide occurrence, in nature, as an important industrial product and problematic scaling mineral.

Filtration studies about calcium carbonate have been performed and are reported in the literature, for example by Wakeman and Tarleton[8] concerning the calcium carbonate

polymorphs aragonite and calcite. However to the author's knowledge there is not one single study about calcium carbonate concerning both the field of crystallization and filtration. This article is an attempt at bridging the gap between crystallization and filtration of calcium carbonate. The questions treated in this article are listed in the following. First the question is treated in which way calcium carbonate morphology and the onset of nucleation affect suspension filterability. For the industrial relevant aromatic amine compound described in Refs. 14 and 15 it was not possible to crystallize plate-like crystals in sufficient amounts for filtration testing. Thus to study the filtration behavior of platelet-like particles as compared to other particle shapes efforts were undertaken to crystallize calcium carbonate exhibiting this plate-like morphology. Needle-like and spherical particle morphologies of L-glutamic acid were investigated according to their filtration behavior in Ref. 15. To compare these particle morphologies with respect to their filtration behavior to a system of another chemical compound it was also aimed at producing these specific particle morphologies for calcium carbonate. Other important questions treated in this section are: what is the influence of crystal size on filtration behavior? In what way do supersaturation, stirring speed and calcium carbonate concentration affect crystal growth, nucleation and as a consequence filtration behavior? To investigate the answers to these questions batch and semibatch reaction crystallization experiments have been performed at varying experimental conditions using both seeded and unseeded strategies.

Experimental

Crystallization experiments

The crystallization experiments to produce different crystal shapes and sizes of $CaCO_3$ were carried out in stirred aqueous solutions in a two 2 L stirred reactor, either in batch experiments or semibatch experiments. The experimental setups for both batch- and semibatch experiments are illustrated in Refs. 17 and 18.

According to the procedure described in Ref. 17, adding an aqueous solution of 0.2 M K_2CO_3 (1 L; Sigma-Aldrich, $\geq$99%) to a stirred (2000 rpm) solution of 0.2 M (1 L) $Ca(CH_3COO)_2{\cdot}H_2O$ (Sigma-Aldrich, $\geq$99) at 30°C allowed for the production of spherical seed crystals of the vaterite polymorph (7–8 μm). These unseeded batch experiments were performed at a temperature of 30°C to obtain a high yield of spherical vaterite crystals. This becomes evident from the work of Ogino et al.[19] which shows that the initial composition of polymorphs arising from the amorphous precursor depends on the crystallization temperature. The crystallization process was finished after 15 min to avoid transformation of vaterite to a more stable polymorph. Crystallization was stopped by separating the crystals from the aqueous solution by filtration. After filtration the particles were washed with ethanol and then dried at 100°C.

The supersaturation ratio, S, defined by Eq. 10 was calculated by Eq. 11 for spherical vaterite crystals because these particles were formed from initially forming amorphous calcium carbonate.[20]

$$S = \sqrt{\frac{a_{Ca^{2+}}\, a_{CO_3^{2-}}}{K_{sp}}} \tag{10}$$

$$S = \sqrt{\frac{K_{sp,\ amorph}}{K_{sp,\ vaterite}}} \tag{11}$$

In Eqs. 10 and 11 a_{Ca}^{2+} and a_{CO3}^{2-} are the activity of calcium- and carbonate ions, respectively, K_{sp} is the thermodynamic solubility product, and $K_{sp,\ amorph}$ and $K_{sp,\ vaterite}$ are the thermodynamic solubility products of amorphous calcium carbonate and vaterite, respectively. The thermodynamic solubility product of the amorphous phase, $K_{sp,\ amorph}$, was calculated by averaging the values given by Clarkson et al.[21] and Brečević and Nielsen.[20] The thermodynamic solubility product of vaterite was taken from the article of Plummer and Busenberg.[22]

Spherical vaterite particles of a larger size were grown by adding seed crystals to a saturated (with respect to vaterite) Na_2CO_3 solution (0.2 mol; Fluka, $\geq$99%), into which saturated (also with respect to vaterite) $CaCl_2{\cdot}2H_2O$-solution (0.2 mol; Fluka, $\geq$99%) was slowly added by a peristaltic pump. Crystallization was performed at 30°C and at 2000 rpm in those semibatch experiments. Two different procedures were applied to increase the particle size. In procedure 1 seed crystals produced in unseeded batch experiments were first washed (ethanol) and dried. Then they were used (33 wt % with respect to the expected final solid mass) as seed crystals in a semibatch crystallization experiment. The product crystals from this experiment were again washed, dried and used as seed crystals (33 wt %) in the next semibatch experiment. Several crystallization experiments were performed subsequently by this procedure. This stepwise crystallization allowed for increasing the particle size. Calcium ions were added by an addition rate of 0.1 and 0.2 mol/h in those experiments. In procedure 2 the amount of seed crystal which were produced in unseeded batch experiments was lowered to values below 33 wt % in a one-step procedure. For experiments of procedure 2 the pumping rate was 0.75 mol/h.

Particles of calcite which were roughly cube-shaped were crystallized at 10°C by adding Na_2CO_3 (0.2 M) instantaneously to a solution made of 0.2 M $CaCl_2{\cdot}2H_2O$ and stirring at 300 rpm for 22 h. Crystallization of calcite at room temperature by transformation of the vaterite polymorph would be another way to produce cube-shaped particles of calcite, but the unwanted extent of agglomeration is much higher at that temperature. Therefore a lower temperature of 10°C has been chosen to produce approximately cube-shaped calcite particles. Plate-like particles of calcite were crystallized by adding 0.2 L of a solution containing 0.2 mol $CaCl_2$ and 1.2 mol LiCl (Sigma-Aldrich, $\geq$99) instantaneously to 1.8 L of a solution containing 0.2 mol of Li_2CO_3 (Merck, $\geq$99). The crystallization temperature was 45°C, crystallization time was 64 h and the stirring speed was set to 2000 rpm. Needle-shaped particles of aragonite were crystallized by feeding 0.2 mol of $CaCl_2{\cdot}2H_2O$ to 0.2 mol of Na_2CO_3 within 8.5 h at 90°C at a stirring speed of 500 rpm. A high temperature of 90°C was chosen as it yields nearly pure aragonite. After each crystallization experiment the crystal suspension was filtered, afterwards it was washed with ethanol and then dried at 100°C.

To investigate the influence of the addition rate and supersaturation ratio on the nucleation and filtration behavior of vaterite the addition rate of calcium ions was varied between 0.75 mol/h and 102.86 mol/h (direct addition without pump) in semibatch experiments performed at 30°C and 2000 rpm. The crystallization was finished directly after the calcium ions containing solution was added (0.75 mol/h) or 15 min after the completed addition in the experiment with 102.86 mol/h feed rate, respectively. For the seeded semibatch experiment performed at 0.75 mol/h the initial supersaturation, S_0, was estimated from the second order growth rate relationship[23] (Eq. 12) assuming that neither crystal nucleation nor aggregation occurs.

$$G = k_g (S-1)^2 \tag{12}$$

On the basis of the given growth rate constants in Ref. 23, Eq. 13 which expresses the integrated form for the activation energy, E_a,[23,24] and the universal gas constant, R, the growth rate constant, k_g, at 30°C was calculated to be 0.56 nm/s.

$$E_a = \frac{R\,T_1\,T_2}{T_2 - T_1} \ln \frac{k_{g,2}}{k_{g,1}} \tag{13}$$

The initial growth rate, G_0, was computed by the following general equation for the growth rate, G, which expresses the change in the particle radius with time:

$$G = \frac{\Delta r}{\Delta t} \tag{14}$$

With the help of the total particle volume, V_s, and the total number of particles, N, both measured with the Coulter Counter Multisizer III (Beckman Coulter), the sphere radius, r, could be calculated:

$$r = \sqrt[3]{\frac{3\,V_s}{4\,\pi N}} \tag{15}$$

Particle suspension (1–3 mL) was diluted with ~200 mL saturated aqueous solution before Coulter Counter Multisizer measurements were carried out. Saturated solution was produced by dissolving and stirring vaterite particles (amount in excess to solubility) in an aqueous solution containing 0.15 M $NaNO_3$. After around 1 hour, the suspension was filtered with a filter of 0.22 μm pore size. The filtered solution was then used to dilute samples from the performed crystallization experiments to measure particle size distributions.

The influence of the $CaCO_3$ concentration on the crystal and filtration properties was investigated at 30°C and 2000 rpm for 0.1 and 0.2 mol $CaCO_3$/L. The influence of the stirring speed was investigated for the calcite polymorph of calcium carbonate at a temperature of 30°C. Cube-shaped crystals were obtained by adding 0.2 M Na_2CO_3 instantaneously to 0.2 M of $CaCl_2{\cdot}2H_2O$ at this temperature. The stirring speed was varied between 300 and 2000 rpm in and average specific cake resistance values were determined after the crystallization process.

After each of the above mentioned crystallization experiments the crystal suspension was filtered, and subsequently washed with ethanol and dried at 100°C. Scanning electron microscopy (Zeiss Ultra 55 Limited Edition) and X-ray powder diffraction (Siemens, D-5005 X-Ray) were used to investigate polymorphism and crystal morphology. To find the polymorphic abundance of the calcite polymorph by means of XRD the peak height of the calcite peak at a 2Θ value of 29.5 was compared. The experimentally determined XRD-spectra of vaterite, aragonite and calcite are shown in Ref. 17.

Filtration experiments

Before each filtration experiment 15 g of dried crystalline substance was suspended in 350 g of pure ethanol. Ethanol was chosen as solvent rather than water due the lower boiling point allowing for short drying times, and because the solubility of calcium carbonate is negligible in ethanol. The particle size distribution was determined by the Coulter Counter Multisizer III (Beckman Coulter) and the chord length distribution was determined by focused beam reflectance measurements (FBRM) (Mettler Toledo, M300) operated in the fine resolution mode at a scanning speed of 2 m/s. The Sauter mean diameter D_{32} was obtained from the size distributions (Coulter Counter) by means of Eqs. 3 and 4 subsequent to dilution of 1–3 mL suspension in 200 mL saturated solution. The standard deviation, s_{PSD}, and the coefficient of variation, c_v, for the particle size distributions (PSD) were calculated according to Eqs. 16 and 17.

$$s_{PSD} = \sqrt{\frac{\sum\left((D_i - D_{32})^2\, A_{s,i}\right)}{\sum\left(A_{s,i}\right)}} \tag{16}$$

where D_i is the mean size of particles in the size interval i and $A_{s,i}$ is the surface area of particles within the size range i.

$$c_v\,(\text{Coulter}) = \frac{s_{PSD}}{D_{32}} \tag{17}$$

The mean chord length, L_m, the standard deviation of the chord length distribution, s_{Cld}, and the coefficient of variation, c_v, were calculated according to Eqs. 18–20.

$$L_m = \frac{\sum(M_i\, y_i)}{\sum(y_i)} \tag{18}$$

where M_i is the midpoint chord lengths and y_i is the number of counts/s, y, per interval, i:

$$s_{Cld} = \sqrt{\frac{\sum\left((M_i - L_m)^2\, y_i\right)}{\sum(y_i)}} \tag{19}$$

$$c_v(\text{FBRM}) = \frac{s_{Cld}}{L_m} \tag{20}$$

The suspensions were filtered at 20°C and $\Delta p = 2$ bar pressure difference in a 1-L pressure Nutsche (BHS, TMG 400) with $A = 20$ cm^2 filter area. Filtrate volume, V, and

filtration time, t, were recorded every 0.2 s by a data collection program. The cake porosity, ε, was calculated based on the cake height, h, measured after the filtration experiment, the dry solid mass and the theoretical value for the solid's density, ρ_s, of the respective polymorph of calcium carbonate ($\rho_{s,vaterite} = 2.67$ g/cm^3 (from Kralj et al.[25]); $\rho_{s,aragonite} = 2.93$ g/cm^3 (Nývlt and Ulrich, 1995[26]), $\rho_{s,calcite} = 2.71$ g/cm^3) according to Eq. 21.

$$\varepsilon = \frac{A\,h - \frac{m_s}{\rho_s}}{A\,h} \tag{21}$$

The dynamic viscosity, η, was determined for pure ethanol and the effective solids concentration, c_s, in kg per m^3 filtrate was determined according to Eq. 22[8]

$$c_s = \rho_l / \left(\frac{1}{s} - \left(1 + \frac{\rho_l}{\rho_s} \frac{\varepsilon}{(1-\varepsilon)} \right) \right) \tag{22}$$

where ρ_l or ρ_s are the density of the liquid or solids, respectively, ε is the cake porosity and s is the mass fraction of solids in the feed suspension.

After combination of Eqs. 8 and 9 the specific average cake resistance could be calculated from the slope of the plot V-t/V and the following equation:

$$\frac{t}{V} = \alpha_V \frac{\eta\, c_s}{2\, A^2 \Delta p} \frac{1}{\rho_s\,(1-\varepsilon)}\, V + \frac{\eta\, \beta}{A\, \Delta p} \tag{23}$$

Equation 7 which is derived from the Carman-Kozeny equation was used to illustrate the effect of the particle size on suspension filterability of spherical particles. Equation 7 was then also used in rearranged form (Eq. 24) to illustrate the effect of crystal size and shape on the specific average cake resistance α_V.

$$\alpha_V^{-0.5} = \Psi\, D_{32} \frac{\sqrt{\varepsilon^3} * 1/6}{(1-\varepsilon)\sqrt{C}} \tag{24}$$

In this equation, C is the Carman-Kozeny constant, ψ is the shape factor, ε is the porosity and D_{32} is the Sauter mean diameter. Although not based on mechanistic reasoning the Sauter mean diameter was also replaced by the mean chord length, L_m, (Eqs. 7 and 24) to demonstrate the relationship between the measured cake resistance values and FBRM measurements.

After filtration the crystals were dried at 100°C and resuspended in ethanol, the particle size and chord length distributions were measured before these crystals were filtered again in the next filtration experiment. This cycle of drying, resuspending, measuring particle characteristics and filtration was repeated three times for all crystal types.

Results and Discussion

Influence of crystal shape and nucleation on filtration behavior

Crystallization. It was possible to crystallize spherical particles of the vaterite polymorph by adjusting the temperature to 30°C during the crystallization experiments (particles from this experiment exp. $CaCO_3$ 1 are shown later in the section "Influence of Initial CaCO3 Concentration on Filtration Behavior"). Analysis by means of XRD has identified the spherical particles as the vaterite polymorph of calcium carbonate and has revealed that less than ~5% of calcite nucleate and grow along with the vaterite polymorph (see also Ref. 18). Different size classes of spherical vaterite were obtained by the two seeding strategies (procedure 1 and 2) presented in the experimental section. Figure 1a shows spherical crystals of vaterite which were produced by the growth of 33 wt % seed crystals of $D_{32} = 7$ μm by adding 0.2 mol Ca^{2+} in the course of 1 hour (exp. $CaCO_3$ 2). It can be seen from Figure 1a that the level of nucleation of new crystals is very small in this experiment. For higher addition rates of 0.75 mol Ca^{2+}/h the nucleation rate was found to be low in all experiments in which seed crystals (according to procedure 1) of sizes (D_{32}) 9.6 μm and lower were used. As a further example, Figure 1b shows crystals grown from crystal seeds with a mean size of approximately $D_{32} =$ 9.6 μm. When the size of the seed crystals is further

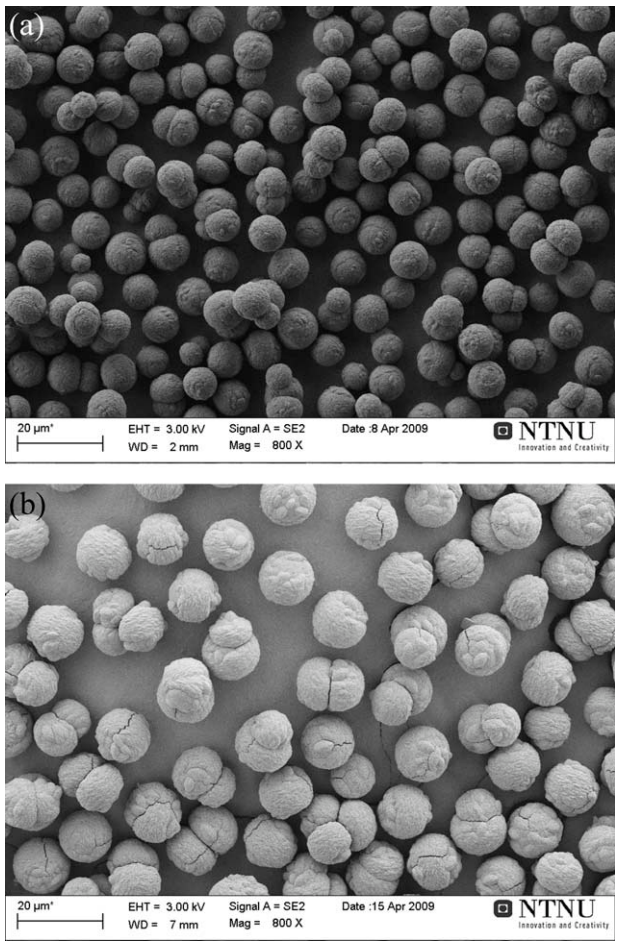

Figure 1. Vaterite crystals grown at 30°C at 2000 rpm at an addition rate of 0.2 mol/h Ca^{2+} from seed crystals (33 wt %) with a Sauter mean diameter of (a) 7 μm (in exp. $CaCO_3$ 2) and (b) D_{32} = 9.6 μm (in exp. $CaCO_3$ 3).

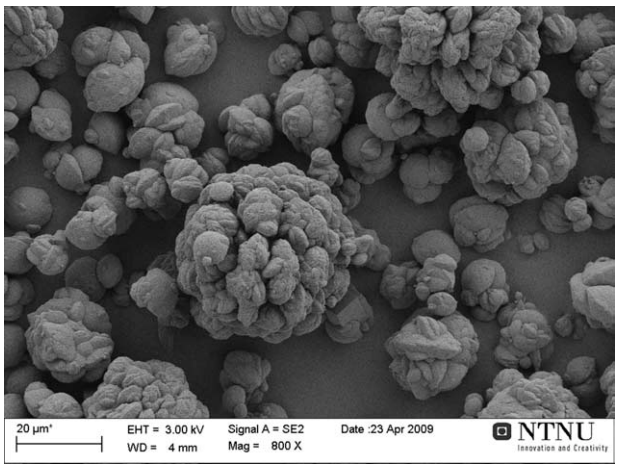

Figure 2. Vaterite crystals (exp. $CaCO_3$ 7) originating from crystal seeds (33 wt %) with a mean size of D_{32} = 23.3 μm grown at an addition rate of 0.1 mol/h Ca^{2+} at 30°C and 2000 rpm.

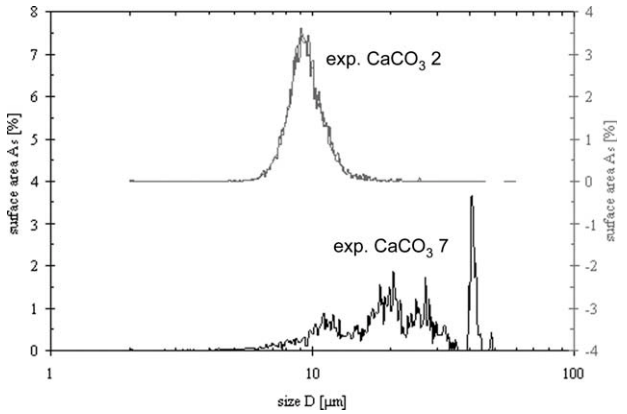

Figure 3. Coulter Counter Multisizer size measurements of vaterite crystals obtained from seed crystals with D_{32} = 7.0 μm (in $CaCO_3$ 2) and D_{32} = 23.3 μm (in $CaCO_3$ 7) at a seed crystal amount of 33 wt %.

increased, the specific surface area of the crystals decreases which leads to the onset of nucleation. Significant nucleation could be observed in exp $CaCO_3$ 7 which can be seen from Figure 2 showing crystals originating from crystal seeds with a mean size of $D_{32} = 23.3$ μm. Though for sparingly soluble salts secondary nucleation is normally marginal as compared to primary nucleation,[27] the secondary nucleation mechanism could play a role in experiments in which larger crystal sizes are observed. In Figure 3 size distributions of particles from exp. $CaCO_3$ 2 measured before subsequently performed filtration experiments are compared to crystals from exp. $CaCO_3$ 7. Besides Figure 2 also the size distribution of particles from $CaCO_3$ 7 indicates a larger number of smaller crystals nucleating and growing during the crystallization experiment. Crystals from this experiments (Table 1) show also a decreased mean size ($D_{32} = 22.03$ μm) as compared to crystals from exp. $CaCO_3$ 6 ($D_{32} = 23.33$ μm). FBRM measurements, on the other hand, show a reduction in the mean chord length already for exp. $CaCO_3$ 6.

The particle size distribution for exp. $CaCO_3$ 2 shows a more uniform shape supporting the conclusion drawn from Figure 1a that calcium and carbonate ions are only consumed by the growing crystals and not by nucleation of new particles.

Chord length distributions which were measured by FBRM (Figure 4) do not reflect the observed width of the size distribution as measured by in the Coulter Counter. This may be attributed to a lower sensitivity of the FBRM measurements for particles in the investigated $CaCO_3$ system. Also the coefficient of variation extracted from the FBRM chord length distributions indicates a lower sensitivity as compared to Coulter Counter measurements as seen from the results shown in Table 1. Thus the interpretation of the filtration results is in the following mainly based on the results obtained from the Coulter Counter measurements.

When the amount of seed crystals is reduced from 33 to 9 wt % in procedure 2 only a small increase in the amount of freshly nucleated crystals can be observed. Accordingly the product crystal size increases due to the lower crystal surface area per unit mass when using lower seed crystal amounts. At a seed amount of 1 wt %, however, the magnitude of nucleation is significant.[18] XRD-analyis showed that the nucleating polymorph in this case is not vaterite, as could be expected from the other experiments performed with vaterite seeds, but calcite. In the case 1 wt % seed crystals were used secondary nucleation is not supposed to play a significant role since the crystal structure of the nucleating polymorph is different from that of the seed crystals. Filtration experiments are not shown for this experiment because of the observed mixture of shapes.

Table 1. Crystal Characteristics of Selected Experiments of Spherical, Needle-Like, Plate-Like and Spherulitic, Cube-Like Particles Measured Before Filtration Testing

Experiment	Feed Rate f_r (mol h^{-1})	Sauter Mean Diameter D_{32} (μm)	Mean Chord Length L_m (μm)	Coefficient of Variation c_v (Coulter) (---)	Coefficient of Variation c_v (FBRM) (---)
$CaCO_3$ 2	0.2	9.61 ± 0.08	13.08 ± 0.03	0.19 ± 0.02	0.79 ± 0.00
$CaCO_3$ 3	0.2	13.22 ± 0.04	14.94 ± 0.08	0.13 ± 0.00	0.78 ± 0.00
$CaCO_3$ 5	0.1	22.20 ± 0.11	22.14 ± 0.25	0.32 ± 0.01	0.67 ± 0.00
$CaCO_3$ 6	0.1	23.33 ± ---	21.54 ± ---	0.45 ± ---	0.73 ± ---
$CaCO_3$ 7	0.1	22.03 ± ---	21.06 ± ---	0.48 ± ---	0.76 ± ---
$CaCO_3$ 8 (plates)	---	14.27 ± 0.09	18.42 ± 0.21	0.28 ± 0.00	0.81 ± 0.01
$CaCO_3$ 9 (cubes)	---	16.18 ± 0.33	19.70 ± 0.26	0.24 ± 0.00	0.74 ± 0.01
$CaCO_3$ 10 (needles)	---	17.16 ± 1.47	12.88 ± 0.49	0.41 ± 0.01	0.92 ± 0.00

Exp. $CaCO_3$ 4 is not shown.

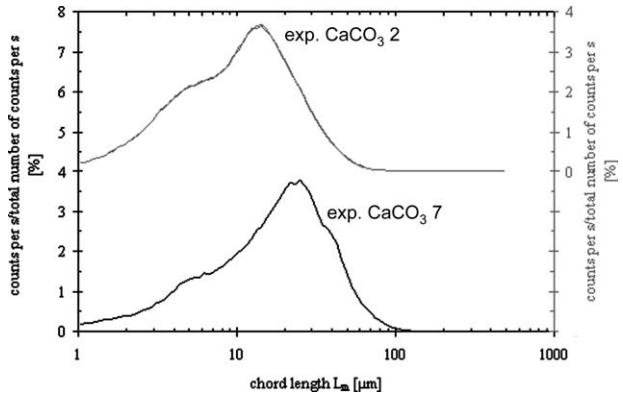

Figure 4. FBRM measurements of vaterite crystals obtained before the filtration experiments.

The crystallization experiments were performed with seed crystals of $D_{32} = 7.0$ μm ($CaCO_3$ 2) and $D_{32} = 23.3$ μm ($CaCO_3$ 7).

According to the experimental procedures described in experimental section it was possible to produce the calcite polymorph in different morphologies. The calcite morphology (Figure 5) which is also shown in Ref. 18 has, to the author's knowledge, not been shown before in the literature. The plate-like morphology with hexagonal features could only be obtained under the influence of significant levels of Li^+. The spherulitic, cube-shaped crystals of calcite are shown in Figure 6. Precipitation at room temperature resulted in smooth calcite polyhedra, but the unwanted extent of agglomeration is much higher at that temperature. Needle-shaped particles (Figure 7) could be obtained at low supersaturation and high temperature. In this experiment, low supersaturation during the crystallization process was obtained by a slow addition of Ca^{2+}. In Figure 8 the particle size distributions (Coulter Counter Multisizer III) of the investigated particle morphologies of calcium carbonate are displayed.

Filtration. The influence of the Sauter mean diameter, D_{32}, on the specific average cake resistance α_v is illustrated in Figure 9 for spheres of vaterite obtained by procedure 1 and 2 (black solid line) with a coefficient of variation c_v (Coulter Counter) lying between the limits of 0.13 and 0.19 and a porosity of $\varepsilon = 0.53$ to 0.59. Limits for the coefficient of variation and the porosity were chosen as both parameters supposedly also affect the magnitude of the Carman-Kozeny constant. The examples exp. $CaCO_3$ 2 and exp. $CaCO_3$ 3 show that spherical particles with a Sauter mean diameter of 9.61 μm (see also Table 1) lead to higher values for the average specific cake resistance ($\alpha_v = 5.7 \times 10^{12}$ m^{-2}; see Table 2) than particles of $D_{32} = 13.22$ μm ($\alpha_v = 2.9 \times 10^{12}$ m^{-2}). Exp. $CaCO_3$ 2 and exp. $CaCO_3$ 3 constitute a part of the underlying filtration results displayed in Figure 9 together with experiments produced by procedure 1 and 2 which are lying within the specified limits for the porosity and the coefficient of variation. From the illustration in this figure [data points from (2) to (3)] it can be seen that a decrease in the Sauter mean diameter, D_{32}, leads to worse filterability as can be seen from the increase in α_v. The deviation from the behavior predicted by theoretical calculations based on mono dispersed spheres (ideal spheres, dotted grey line in Figure 9) for which the shape factor ψ equals 1 can be seen from the rise in the factor C/ψ^2 from 5 in the ideal case[7–9] to 9.4. The value of 9.4 was calculated from the

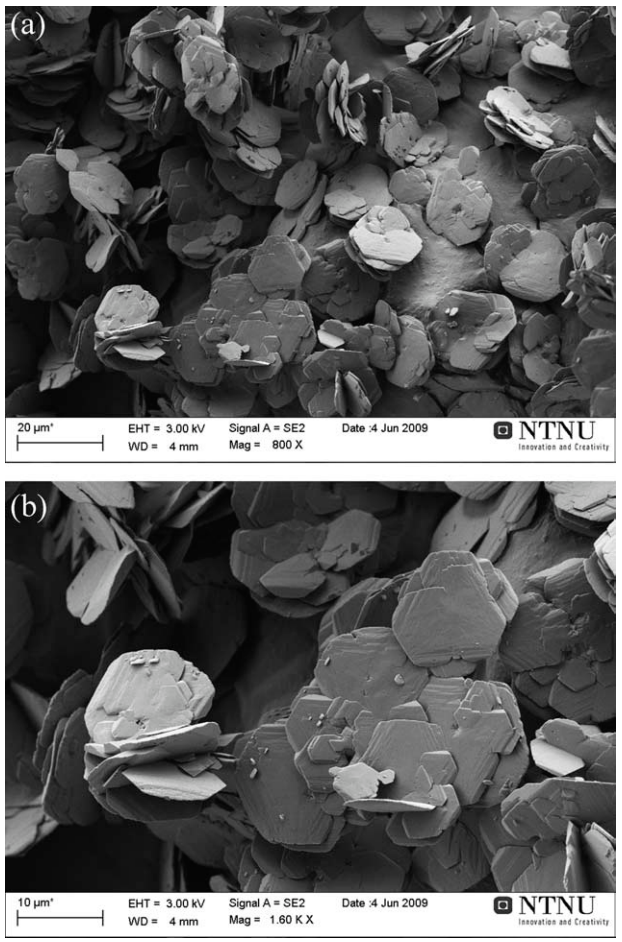

Figure 5. Crystals of calcite from exp. $CaCO_3$ 8: plate-like particles produced at 45°C in the presence of Li^+ at a magnification of (a) 800 and (b) 1600.

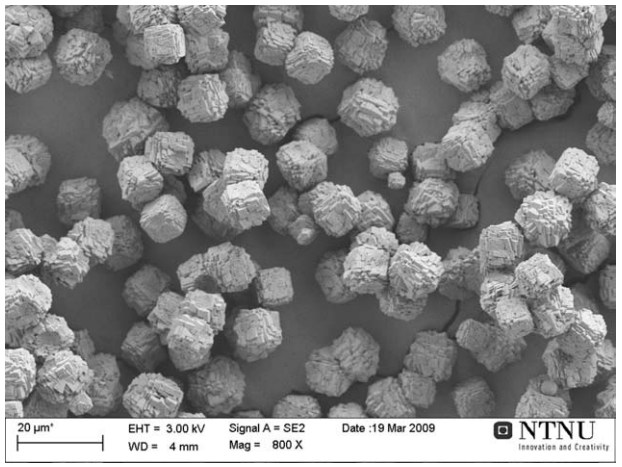

Figure 6. Crystals of calcite from exp. $CaCO_3$ 9: spherulitic, cube-like particles produced at 10°C.

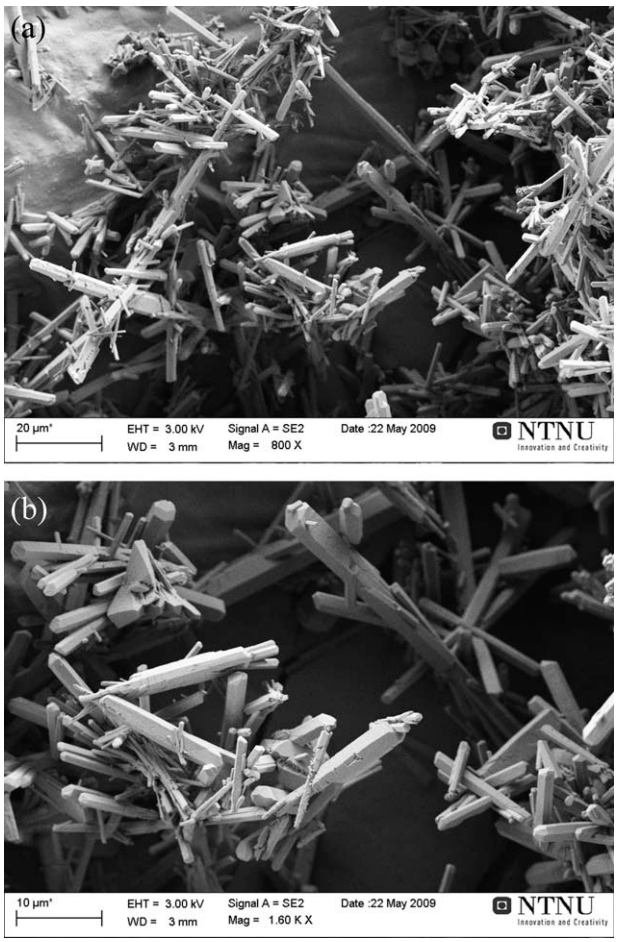

Figure 7. Aragonite polymorph of $CaCO_3$ crystallized as needle-shaped particles at 90°C by slowly adding Ca^{2+} ions to a solution containing CO_3^{2-} ions (exp. $CaCO_3$ 10).

The magnification is 800 in (a) and 1600 in (b).

slope of the regression line for all data points between the points marked with (2) and (3) in Figure 9.

Although there is no theoretical foundation for the connection between L_m and the cake resistance, the aforementioned results can be confirmed (Figure 10): the specific average cake resistance increases with decreasing size. In case of the FBRM measurements, however, the particle size information is represented by the mean chord length, L_m.

First, the increase in C/ψ^2 for the investigated crystals can be explained by the fact that the particles exhibit a size distribution instead of a uniform size which increases the value of C. Second, deviations with regard to the perfectly spherical shape lead to a decrease in the shape factor ψ and therefore play a role in increasing the term C/ψ^2 which accounts for the decreased filterability. The specific cake resistance value for each performed experiment has been recalculated (Eq. 7) for a porosity of $\varepsilon = 0.58$ and the results are shown in Figure 11 based on Eq. 24. The filtration results of spherical crystals of vaterite illustrated in Figure 9 are also shown in the illustrations of Figure 11. Included in this figure are furthermore results of filtration experiments performed with spherical crystals exhibiting wider size distributions. The

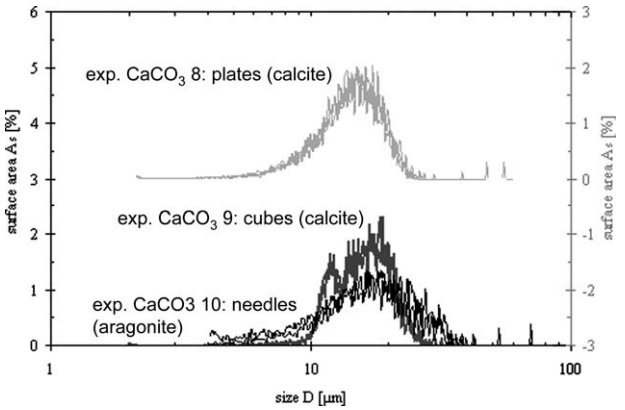

Figure 8. Results of Coulter Counter measurements of plate-like, cube-shaped, and needle-like crystals obtained before filtration testing.

For all particle morphologies three particle size distributions are shown which are resulting from measurements performed before each of the subsequently carried out filtration experiments.

coefficient of variation of the experiments $CaCO_3$ 5, exp. $CaCO_3$ 6 and exp. $CaCO_3$ 7 are $c_v = 0.32$, $c_v = 0.45$, and $c_v = 0.48$ (Table 1). Comparing exp. $CaCO_3$ 5 with exp. $CaCO_3$ 6 the mean size increases from $D_{32} = 22.2$ μm to $D_{32} = 23.3$ μm in exp. $CaCO_3$ 6. However the measured specific cake resistance value does not decrease significantly as would be expected considering the increase in the Sauter mean diameter. Introducing large crystal seeds of $D_{32} = 23.3$ μm in exp. $CaCO_3$ 7 even yields product crystals of smaller particle size ($D_{32} = 22.03$ μm) comparable to the size of crystals from exp. $CaCO_3$ 5. The particle size reduction has been explained by the onset of significant nucleation throughout the crystallization experiment. It is proposed that both the decrease in D_{32} (exp. $CaCO_3$ 6 and exp. $CaCO_3$ 7)

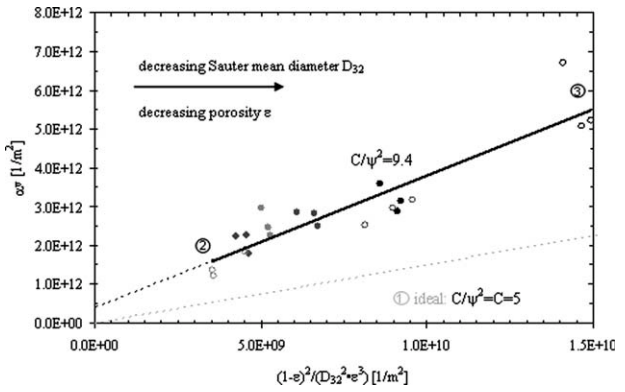

Figure 9. Average specific cake resistance α_v as a function of the porosity ε and the Sauter mean diameter D_{32} for spherical crystals of the vaterite polymorph of $CaCO_3$ obtained by procedure 1 and 2.

Experiments shown in this figure exhibit a coefficient of variation of 0.13–0.19 and a porosity of 0.53–0.59. The black solid line represents a linear fit of the displayed results. The plot based on the Carman-Kozeny equation shows that the specific cake resistance increases with decreasing Sauter mean diameter, and with decreasing porosity.

Table 2. Filtration Characteristics of the Experiments Shown in Table 1

Experiment	Porosity ε (---)	Cake Resistance α_m (m kg^{-1})	Cake Resistance α_v (m^{-2})	Constant C/Ψ^2 (---)
$CaCO_3$ 2	0.54 ± 0.00	$4.6 \times 10^9 \pm 7.7 \times 10^8$	$5.7 \times 10^{12} \pm 9.0 \times 10^{11}$	10.8
$CaCO_3$ 3	0.53 ± 0.01	$2.3 \times 10^9 \pm 2.3 \times 10^8$	$2.9 \times 10^{12} \pm 3.4 \times 10^{11}$	9.0
$CaCO_3$ 5	0.57 ± 0.04	$1.4 \times 10^9 \pm 8.4 \times 10^7$	$1.6 \times 10^{12} \pm 3.5 \times 10^{10}$	22.6
$CaCO_3$ 6	0.54 ± 0.00	$1.6 \times 10^9 \pm$ ---	$2.0 \times 10^{12} \pm$ ---	22.2
$CaCO_3$ 7	0.54 ± 0.00	$2.8 \times 10^9 \pm$ ---	$3.4 \times 10^{12} \pm$ ---	35.5
$CaCO_3$ 8 (plates)	0.70 ± 0.01	$2.2 \times 10^9 \pm 2.3 \times 10^8$	$1.8 \times 10^{12} \pm 1.5 \times 10^{11}$	40.0
$CaCO_3$ 9 (cubes)	0.65 ± 0.01	$9.8 \times 10^8 \pm 2.6 \times 10^8$	$9.4 \times 10^{11} \pm 2.6 \times 10^{11}$	14.9
$CaCO_3$ 10 (needles)	0.86 ± 0.01	$8.2 \times 10^8 \pm 4.5 \times 10^8$	$3.4 \times 10^{11} \pm 2.2 \times 10^{11}$	83.6

as well as the increasing width of the size distribution (exp. $CaCO_3$ 5 as compared to exp. $CaCO_3$ 7) reduce the filterability of the investigated crystal suspensions (Table 2). The larger width of the size distribution for exp. $CaCO_3$ 7 coheres with a larger value for the term C/ψ^2 being 22.6 for exp. $CaCO_3$ 5 and 35.5 for exp. $CaCO_3$ 7. Thus these results show that filterability decreases due to crystal nucleation when the seed crystal size exceeds a certain value. Table 2 also shows that the porosity is not significantly different when comparing experiments $CaCO_3$ 2-$CaCO_3$ 7. This means that the width of the size distribution does not affect porosity to a large extent in these experiments, as would for example be the case if smaller particles were migrating into larger pores within the filter cake. It can therefore be proposed that the observed deterioration of suspension filterability as a consequence of a broader size distribution is mainly caused by a change of the flow pattern within the filter cake which affects the Carman-Kozeny constant.

On the other hand the obtained results (Tables 1 and 2) show that suspension filterability increases with increasing seed crystal size unless a certain seed crystal size at which significant nucleation occurs is reached. The increase of filterability with increasing seed size can be explained by a lower number of particles on which surface calcium carbonate can grow when large seed crystals are used.

The close distance of the measurement points for spherulitic cubes (exp. $CaCO_3$ 9) to the trendline of vaterite spheres (Figure 11) shows that the filterability of spheres and cubes is in the same range. This is also shown by the term C/ψ^2 which was calculated to be 14.9 for cube-like crystals (Table 2). Plate-like crystals of exp. $CaCO_3$ 8 give a value of 40 for C/ψ^2 indicating low filterability. The higher value of C/ψ^2 for plates as compared to spheres can be explained by a lower value for the shape factor ψ in this case due to the high specific surface area of plate-like particles.[8]

For needle-like crystals of exp. $CaCO_3$ 10 C/ψ^2 was found to be highest ($C/\psi^2 = 83.6$). Qualitatively, the higher value of C/ψ^2 as compared to spherical particles of $CaCO_3$ can be explained by a larger surface area (lower ψ) of the needles. However, the fact that C/ψ^2 is higher for needles than for plates which exhibit a lower value for the shape factor ψ than needles[8] supports the suggestion that also C is increased in case of needle-like crystals. First, the large coefficient of variation of 0.41 for needles indicates that the width of the size distribution increases the constant C. Second, fibrous particles with a high aspect ratio have been reported to ball up or mat on the filter cloth during filtration, possibly leading to higher cake resistance values.[8] And finally, also porosity which is comparatively high for the investigated needle-like crystals may play a role as for the constant C. Beck et al.[15] have also shown that the cake resistance of needle-like crystals of L-glutamic acid is higher than for polyhedral crystals with approximately the same mean chord length. The high standard deviation in the measured mean diameter D_{32} (Figure 11) furthermore indicates that the investigated needle-like crystals are susceptible to breakage which leads

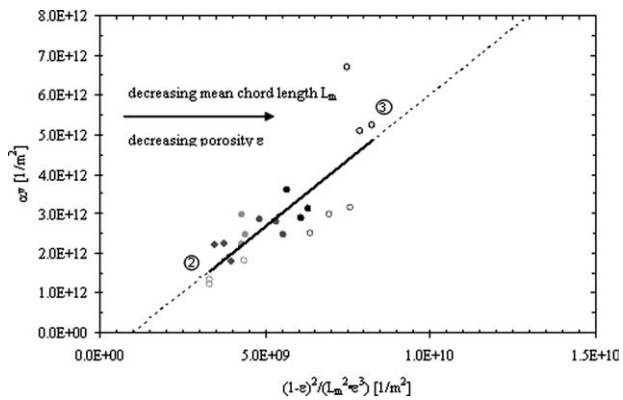

Figure 10. Average specific cake resistance α_v as a function of the porosity ε and the mean chord length L_m for spherical crystals of the vaterite polymorph of $CaCO_3$.

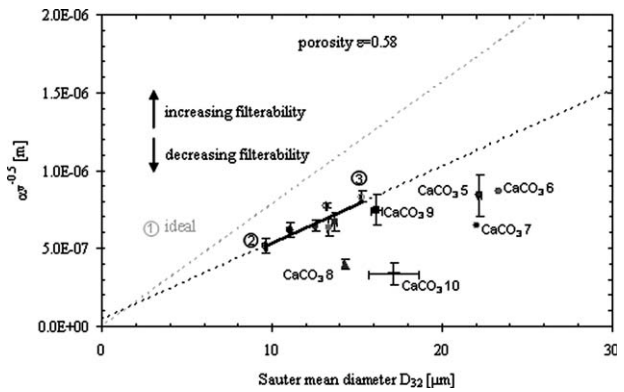

Figure 11. Average specific cake resistance as a function of the Sauter mean diameter D_{32} for spherical particles of $CaCO_3$ of different sizes (2-3) and distributions ($CaCO_3$ 5-$CaCO_3$ 7), plates ($CaCO_3$ 8), cubical particles ($CaCO_3$ 9) and needles ($CaCO_3$ 10), recalculated for a porosity of $\varepsilon = 0.58$.

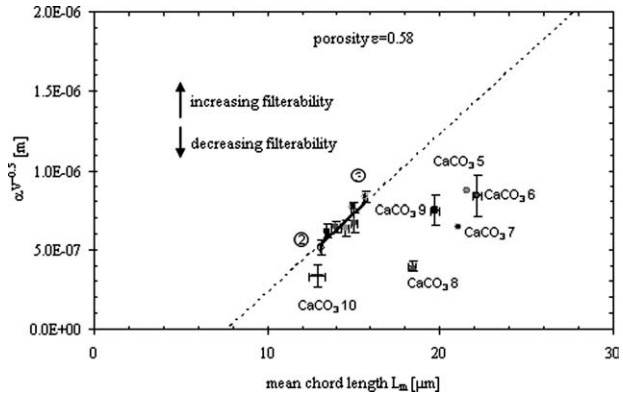

Figure 12. Average specific cake resistance as a function of the mean chord length L_m for spherical particles of $CaCO_3$ of different sizes (2-3) and distributions ($CaCO_3$ 5-$CaCO_3$ 7), plates ($CaCO_3$ 8), cubical particles ($CaCO_3$ 9) and needles ($CaCO_3$ 10) recalculated for a porosity of $\varepsilon = 0.58$.

to comparatively higher values for the cake resistance of needles. Table 2 shows that the high value for C/ψ^2 for needles is often overshadowed by a high cake porosity associated with this particle morphology shifting the measured cake resistance to comparably low values. However, the high cake porosity of needle-like crystals involves also longer drying times which makes this particle morphology industrially less attractive.

As opposed to needle-like crystals, the standard deviation of D_{32} for the other shapes is very low indicating (Table 1) that breakage of spherical, cubical and plate-like crystals due to filtration is negligible. Beck et al.[15] have previously shown that spherical particles of other substances, like L-glutamic acid, give rise to high filtration resistance due to particle compressibility. This is not observed for the vaterite spherulites. Particle compressibility due to disintegration, together with a higher value for the coefficient of variation (FBRM) may be an explanation for the fact that the specific cake resistance value is higher for aromatic amine ($>2.4 \times 10^9$ m/kg) and L-glutamic acid (2.0×10^{10} m/kg) spherulites than for spherical particles from experiment $CaCO_3$ 5 (1.4×10^9 m/kg) with comparable mean chord length.

In Figure 12 the filtration results presented in Figure 11 are shown, however in dependence of the mean chord length, L_m, as measured by FBRM. Although there cannot be established a theoretical foundation for the connection between L_m and the cake resistance by means of Eq. 7, many of the aforementioned results can be confirmed: needles and plates show worse filterability than spheres (points 2-3) and nucleation leads to a decrease in filterability (exp. $CaCO_3$ 5, 6, and 7). This shows that FBRM can be used as a predictive tool for filtration for the investigated size and shape variation performed in this study. However unexpectedly, the difference of the measured mean chord length values of various experiments is measured to be smaller than for the Coulter Counter measurements. This may be explained by the different measurement approaches used for these techniques such as sample dilution before the Coulter Counter measurements.

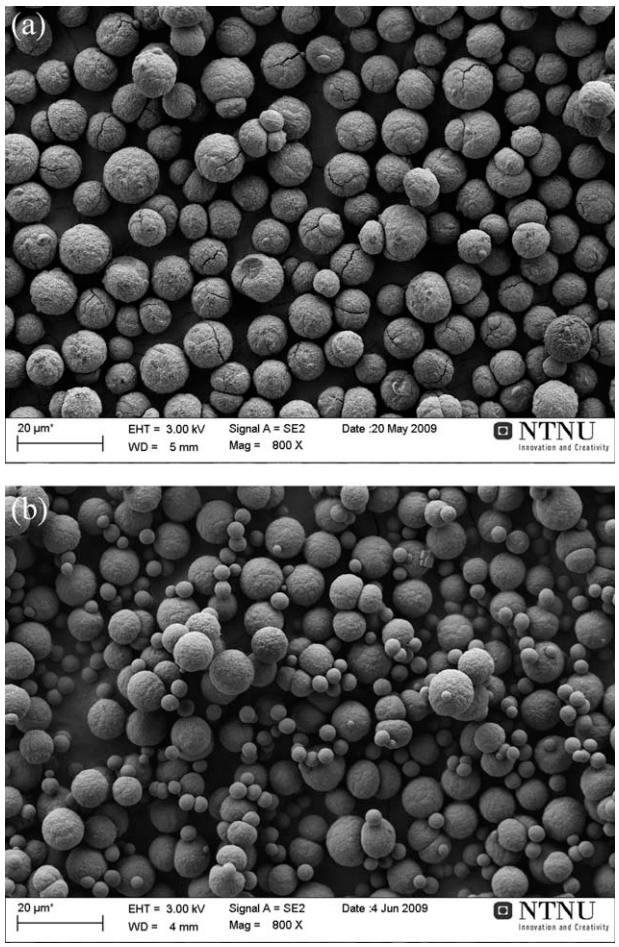

Figure 13. Vaterite crystals grown from seed crystals (33 wt %) at 30°C at 2000 rpm at an addition rate of (a) 0.75 mol/h Ca^{2+} (exp. $CaCO_3$ 11) and (b) 102.9 mol/h Ca^{2+} (exp. $CaCO_3$ 12) to a solution containing CO_3^{2-} ions and seed crystals.

Influence of feed rate and supersaturation on filtration behavior

Spherical vaterite seed crystals were grown both at low (0.75 mol/h) and high feed rate (102.9 mol/h) of calcium

Table 3. Crystal Characteristics for Spherical Vaterite Crystals Grown From Seed Crystals at Low and High Feed Rate

Experiment	Supersaturation Ratio S (---)	Feed Rate f_r (mol h^{-1})	D_{32} for Seed Crystals (μm)	D_{32} for Product Crystals (μm)	D_{32} for Crystals Before Filtration (μm)	L_m for Crystals Before Filtration (μm)	Coefficient of Variation c_v (Coulter)	Coefficient of Variation c_v (FBRM)
$CaCO_3$ 11	3.0	0.75	8.05	10.92	11.04 ± 0.09	13.49 ± 0.07	0.19 ± 0.01	0.80 ± 0.00
$CaCO_3$ 12	S>3.0	102.86	7.89	9.59	9.36 ± 0.09	11.57 ± 0.15	0.31 ± 0.00	0.79 ± 0.01

Table 4. Filtration Characteristics for Spherical Vaterite Crystals Grown From Seed Crystals at Low and High Feed Rate

Experiment	Porosity ε (---)	Cake Resistance α_m (m kg^{-1})	Cake Resistance α_v (m^{-2})	Constant C/Ψ^2 (---)
$CaCO_3$ 11	0.56 ± 0.00	$2.7 \times 10^9 \pm 3.3 \times 10^8$	$3.2 \times 10^{12} \pm 3.6 \times 10^{11}$	9.9
$CaCO_3$ 12	0.61 ± 0.01	$6.5 \times 10^9 \pm 2.7 \times 10^8$	$6.8 \times 10^{12} \pm 4.1 \times 10^{11}$	24.5

ions to a saturated solution containing carbonate ions and crystals seeds. The results of these experiments are shown in Figure 13a (exp. $CaCO_3$ 11) and Figure 13b (exp. $CaCO_3$ 12). In Figure 13b it can be seen that the number of freshly nucleated vaterite crystals is significant in experiment exp. $CaCO_3$ 12 in which the feed rate was set to a high value. The onset of significant nucleation throughout the crystallization process of this experiment can be explained by a higher supersaturation ratio associated with the high feed rate. The supersaturation ratio is thus significantly larger in exp. $CaCO_3$ 12 than $S = 3$ calculated for exp. $CaCO_3$ 11. Nucleation of crystals in exp. $CaCO_3$ 12 also influences the measured particle size, mean chord length and coefficient of variation. Table 3 shows that D_{32}, L_m are lower whereas c_v (Coulter Counter) is larger for exp. $CaCO_3$ 12. The coefficient of variation from the FBRM measurements is only insignificantly higher for exp. $CaCO_3$ 12, but as mentioned before this is attributed to a lower sensitivity of the FBRM measurements in this particle system. The influence of the crystal properties displayed by the crystals produced in exp. $CaCO_3$ 11 and exp. $CaCO_3$ 12 are illustrated in Table 4. This table clearly shows that nucleation of crystals throughout the crystallization process leads to higher values for the cake resistance. The increase in the average specific cake resistance is caused by the lower product crystal size of exp. $CaCO_3$ 12 and the wider size distribution (larger c_v) which increases the term C/Ψ^2. The experiments show that it is crucial to control the level of supersaturation during the process of crystallization so as to guarantee good filtration behavior in the subsequent solid-liquid separation stage. This observation is in accordance with Mullin who shows[24] that increasing the supersaturation leads to an increase in both the nucleation and crystal growth rate. At a high supersaturation, nucleation of new crystals dominates over crystal growth. The consequence of this is that high supersaturation levels lead to small crystals, normally also exhibiting a broad particle size distribution. Scientific contributions dealing with the control of supersaturation and crystallization processes in general, can be found in Refs. 28–35.

Influence of initial $CaCO_3$ concentration on filtration behavior

Spontaneous precipitation experiments of calcium carbonate were performed at low (0.1 mol $CaCO_3$/L) and high calcium carbonate concentration (0.2 mo/L). The results of these experiments are shown in Figure 14a (exp. $CaCO_3$ 1 and Figure 14b (exp. $CaCO_3$ 13). Comparing these figures it becomes evident that vaterite crystals are smaller when the initial calcium carbonate concentration is comparably high. Both Coulter Counter and FBRM measurements verified the smaller particle size of crystals precipitated at higher calcium carbonate concentration (Table 5). The supersaturation ratio is $S = 7.1$ in both experiments since the vaterite spheres crystallized from the amorphous precursor compound (see Experimental Section). The reason for the smaller particle size of crystals obtained in exp. $CaCO_3$ 13 may be accounted for by a higher heterogeneous nucleation rate for vaterite due to a larger amount of amorphous precursor substance. The coefficient of variation (Coulter Counter) is slightly higher for particles from exp. $CaCO_3$ 13 ($c_v = 0.32$) as compared to exp. $CaCO_3$ 1 ($c_v = 0.29$). The average specific cake resistance is found to be higher for particles produced at higher calcium carbonate concentration ($\alpha_v = 1.5 \times 10^{13}$ m^{-2}) than for crystals from exp. $CaCO_3$ 1 ($\alpha_v = 9.9 \times 10^{12}$ m^{-2}). These findings can be explained by the lower

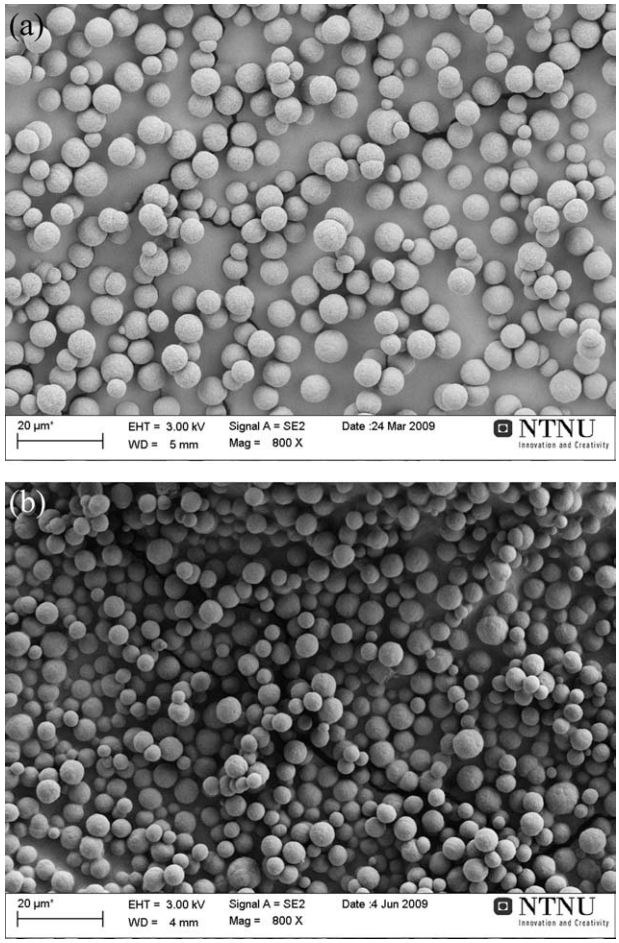

Figure 14. Vaterite crystals grown from the amorphous precursor phase at a temperature of 30°C at 2000 rpm.

The crystallization time was 15 min. The calcium carbonate concentration was 0.1 mol/L in (a) (exp. $CaCO_3$ 1), and 0.2 mol/L in (b) (exp. $CaCO_3$ 13).

Table 5. Crystal Characteristics for Spherical Vaterite Crystals Grown at Low and High Initial Calcium Carbonate Concentration at $S = 7.1$

Experiment	Concentration of $CaCO_3$ c_{CaCO3} (mol/l)	Sauter Mean Diameter D_{32} for Crystals Before Filtration (μm)	Mean Chord Length L_m for Crystals Before Filtration (μm)	Coefficient of Variation c_v (Coulter) (---)	Coefficient of Variation c_v (FBRM) (---)
$CaCO_3$ 1	0.1	6.99 ± 0.01	9.63 ± 0.03	0.29 ± 0.00	0.81 ± 0.01
$CaCO_3$ 13	0.2	6.03 ± 0.00	8.38 ± 0.07	0.32 ± 0.00	0.79 ± 0.01

Table 6. Filtration Characteristics for Spherical Vaterite Crystals Grown at Low and High Initial Calcium Carbonate Concentration at $S = 7.1$

Experiment	Porosity ε (---)	Cake Resistance α_m (m kg^{-1})	Cake Resistance α_v (m^{-2})	Constant C/Ψ^2 (---)
$CaCO_3$ 1	0.62 ± 0.01	$9.7 \times 10^9 \pm 2.6 \times 10^8$	$9.9 \times 10^{12} \pm 4.9 \times 10^{11}$	21.7
$CaCO_3$ 13	0.63 ± 0.00	$1.5 \times 10^{10} \pm 5.1 \times 10^8$	$1.5 \times 10^{13} \pm 4.6 \times 10^{11}$	26.8

Sauter mean diameter and mean chord length, and slightly higher C/Ψ^2 (see Table 6) of particles precipitated in exp. $CaCO_3$ 13.

Influence of stirring speed on filtration behavior

Unlike spherulitic, cube-shaped crystals of calcite which are shown in Figure 6, the cubical calcite particles shown in Figure 15 are produced at a higher temperature (30°C) which results in a comparably smoother morphology. However the extent of aggregation is much higher at 30°C. As a comparison to the crystals depicted in Figure 15, the following figure (Figure 16) shows how larger calcite cubes have grown along with nucleated smaller sized cubes in experiment exp. $CaCO_3$ 15 which was performed at 2000 rpm. The onset of nucleation at 2000 rpm is converse to the observations made for vaterite grown at the same temperature of 30°C and may therefore be accounted for by differences in the nucleation behavior of the polymorphic forms. XRD-analysis showed that the resulting crystals in exp. $CaCO_3$ 14 and exp. $CaCO_3$ 15 are 100% calcite.

Coulter Counter size measurements, illustrated in Figure 17 verify the onset of nucleation at high agitation speeds. Nucleation of crystals in exp. $CaCO_3$ 15 during the crystallization process also influences the measured particle size, mean chord length and coefficient of variation. Table 7 shows that D_{32}, L_m are lower whereas c_v is larger for exp. $CaCO_3$ 15. Table 8 indicates that nucleation of crystals throughout the crystallization process leads to higher values for the cake resistance. The increase in the average specific cake resistance is caused by the lower product crystal size of exp. $CaCO_3$ 15 and the wider size distribution (larger c_v) which influences the average cake porosity to decrease from 0.69 in exp. $CaCO_3$ 14 to 0.49 in $CaCO_3$ 15. The experiments show that it is crucial to find an appropriate agitation speed throughout the crystallization process to account for good solid-liquid separation.

Summary and Conclusions

In stirred reaction crystallization experiments of calcium carbonate in aqueous solutions the temperature, supersaturation, seeding procedure and other parameters were varied to control particle size, size distribution and morphology of the particles. The effects of these particle characteristics on filtration behavior were tested in lab-scale cake filtration experiments performed at a constant pressure difference of 2 bar.

Crystals of $CaCO_3$ could be crystallized as spherical polycrystalline particles of the vaterite polymorph, needle-like crystals of aragonite and both cube-like and novel plate-like crystals of calcite. The mean diameter and the size distribution of vaterite spherulites were varied by applying seeding strategies in semibatch experiments. Thereby, saturated solutions of Ca^{2+} were pumped in to saturated solutions of CO_3^{2-} including seed crystals. By changing the amount and size of the seed crystals, and the supersaturation ratio it was possible to control crystal size, and the width of the size distribution by allowing for crystal nucleation. The crystals were resuspended in ethanol, filtered, and then the specific average cake resistance was calculated to describe the filterability of the crystal suspensions. Assuming applicability of the Carman-Kozeny equation the filterability was found to

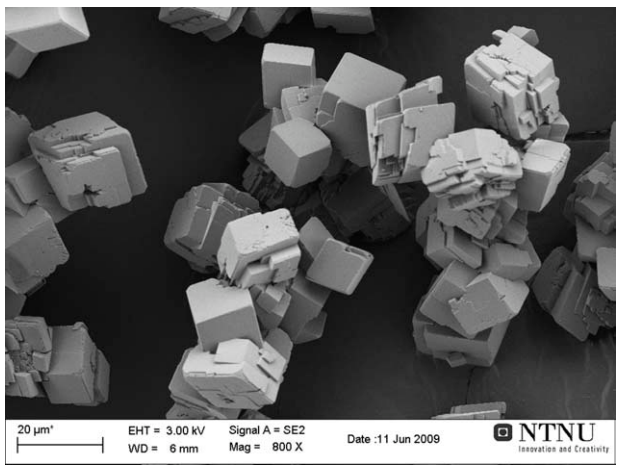

Figure 15. Calcite crystals grown from the metastable vaterite polymorph at a temperature of 30°C at 300 rpm (exp. $CaCO_3$ 14).

The crystallization time was 22 hours.

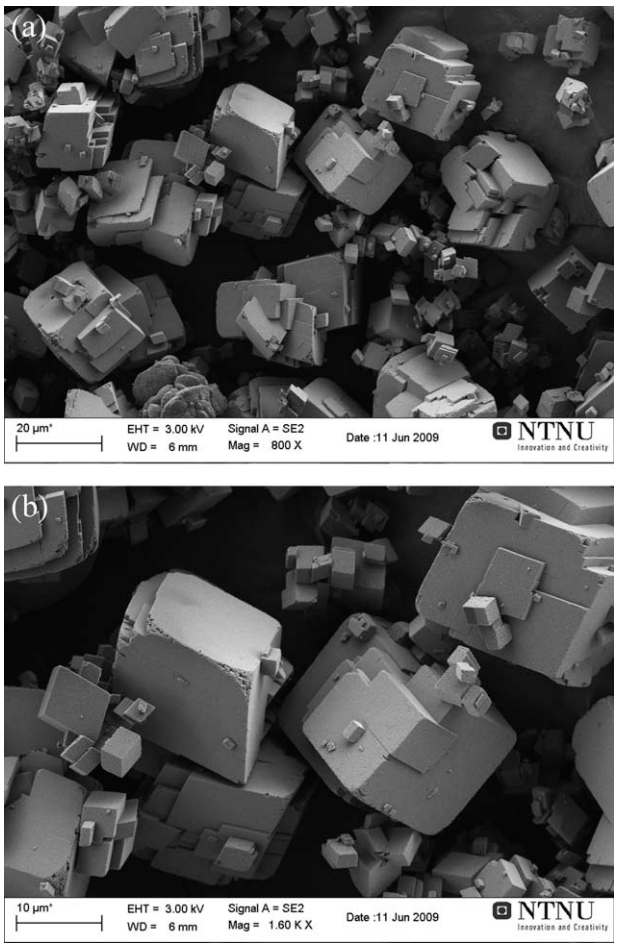

Figure 16. Calcite crystals grown from the metastable vaterite polymorph at a temperature of 30°C at a stirring speed of 2000 rpm (exp. $CaCO_3$ 15).

The crystallization time was 22 hours. The magnification is 800 in (a) and 1600 in (b).

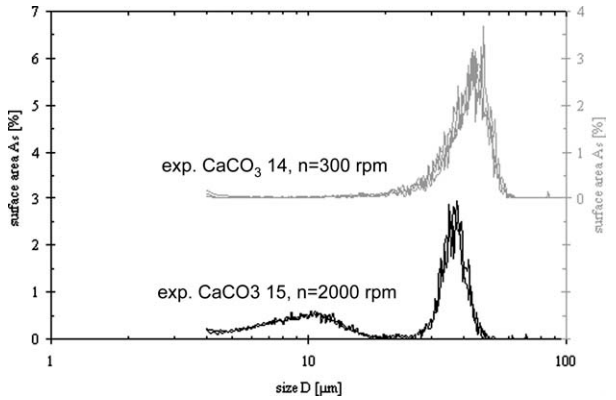

Figure 17. Results of Coulter Counter measurements of calcite cubes crystallized at low ($CaCO_3$ 14) and high ($CaCO_3$ 15) stirring speed.

In all cases three particle size distributions are shown which are resulting from measurements performed before each of the subsequently carried out filtration experiments.

be higher for spherical crystals of $CaCO_3$ with $C/\psi^2 = 9$ than for ideal spheres ($C/\psi^2 = 5$). This deviation from the ideal case can be attributed to the fact that spherical particles of $CaCO_3$ display a particle size distribution rather than a uniform size and smaller variations in the shape as compared to ideal spheres. Smaller spherical particles produced in seeded semibatch experiments as a result of nucleation of new crystals at higher supersaturation ratio were found to result in higher values for the specific average cake resistance. Like higher supersaturation ratios achieved by high feed rates, also seed crystals with a larger size caused the onset of nucleation in seeded semibatch crystallization experiments, and the filterability of the obtained crystal suspensions was found to be deteriorated as a result of a broader particle size distribution. Crystal suspensions stemming from seeded crystallization experiments in which nucleation did not occur showed that the suspension filterability increased with increasing particle size. For the calcite polymorph it was also shown that an increase in the stirring speed leads to nucleation of smaller crystals which in turn decreases suspension filterability.

At a normalized porosity of 0.58, plate-like crystals ($C/\psi^2 = 40$) and needle-like crystals ($C/\psi^2 = 84$) show worse filterability than spherical particles and cube-like particles ($C/\psi^2 = 15$). This observation can be explained by the higher specific surface area of plate-like crystals and needle-like

Table 7. Crystal Characteristics for Cube-Like Calcite Crystals Produced at Low ($CaCO_3$ 14) and High ($CaCO_3$ 15) Stirring Speed

Experiment	Stirring Speed n (rpm)	Sauter Mean Diameter D_{32} for Crystals Before Filtration (μm)	Mean Chord Length L_m for Crystals Before Filtration (μm)	Coefficient of Variation c_v (Coulter) (---)	Coefficient of Variation c_v (FBRM) (---)
$CaCO_3$ 14	300	39.7 ± 0.6	31.5 ± 0.9	0.3 ± 0.01	0.68 ± 0.01
$CaCO_3$ 15	2000	24.5 ± 0.7	25.0 ± 0.2	0.6 ± 0.03	0.72 ± 0.01

Table 8. Filtration Characteristics for Cube-Like Calcite Crystals Produced at Low ($CaCO_3$ 14) and High ($CaCO_3$ 15) Stirring Speed

Experiment	Porosity ε (---)	Cake Resistance α_m (m kg^{-1})	Cake Resistance α_v (m^{-2})	Constant C/Ψ^2 (---)
$CaCO_3$ 14	0.69 ± 0.01	$3.3 \times 10^8 \pm 7.8 \times 10^7$	$2.8 \times 10^{11} \pm 7.2 \times 10^{10}$	40.8
$CaCO_3$ 15	0.49 ± 0.00	$1.7 \times 10^9 \pm 1.6 \times 10^8$	$2.3 \times 10^{12} \pm 2.3 \times 10^{11}$	11.7

crystals as compared to spheres and cubes, and in case of the needles also based on a wider size distribution. Needle-like particles also show a reduction in the crystal size after filtration as they break more easily than other particle morphologies.

To achieve good filterability of particle suspensions crystallization processes should therefore, when possible, be designed in such a way that stable spherical particles of a large a size as possible and with a narrow size distribution are produced. The size and the size distribution of the crystals can for example be controlled by a seeding strategy in the crystallization step. Moderate supersaturation and the right choice of both seed crystal amount and size minimize nucleation and increase the size of the product crystals, and therefore increase filterability.

Acknowledgments

The authors thank the Norwegian Research Council, GE Healthcare, StatoilHydro, Dyno Nobel, Norcem, and Hydro Aluminium for their financial support.

Notation

A = area of filter medium
A_s = surface area of particles
$A_{s,i}$ = surface area of particles in size interval i
a = activity in mol L^{-1}
C = Carman-Kozeny constant
c_{CaCO_3} = concentration of $CaCO_3$ in mol/L
c_s = effective solids concentration in kg m^{-3}filtrate
c_v = coefficient of variation
D = sphere diameter
D_i = sphere diameter of particles in size interval i
D_{sv} = surface to volume mean size of particles of any shape
D_{32} = Sauter mean diameter
E_a = activation energy in J mol^{-1}
f_r = feed rate in mol h^{-1}
G = growth rate in m s^{-1}
G_0 = initial growth rate in m s^{-1}
h = cake height
K_{sp} = solubility product in mol^2 L^{-2}
k_g = growth rate constant m s^{-1}
L_m = mean FBRM chord length
M_i = midpoint of FBRM chord length of interval i
m_s = mass of dry crystals
n = stirring speed in rpm
N = number of particles
R = universal gas constant
r = sphere radius
S = supersaturation ratio
S_0 = initial supersaturation ratio
S_v = specific surface area in m^2 m^{-3}
s = mass fraction of solids in feed suspension in kg kg^{-1}
s_{PSD} = standard deviation of particle size distribution
s_{CLD} = standard deviation of chord length distribution
T = temperature
t = time
V = filtrate volume
V_s = particle volume
V_{tot} = total cake volume
V_v = voids volume
y_i = number of FBRM counts/s in interval i
α_v = average specific cake resistance in m^{-2}
α_m = average specific cake resistance in m kg^{-1}
β = filter medium resistance in m^{-1}
Δp = pressure difference
ε = porosity
η = dynamic viscosity
ρ_l = density of liquid phase
ρ_s = density of solids
Ψ = shape factor

Literature Cited

1. Wibowo C, Chang W-C, Ng KM. Design of integrated crystallization systems. *AIChE J*. 2001;47:2474–2492.
2. Svarovsky L. *Solid-Liquid Separation*, 4th ed. Oxford: Butterworth-Heinemann, 2000.
3. Carman PC. Fluid flow through granular beds. *T I Chem Eng-Lond*. 1937;15:150–166.
4. Carman PC. Determination of the specific surface of powders, Part I. *J Soc Chem Ind*. 1938;57:225–234.
5. Carman PC. Determination of the specific surface of powders, Part II. *J Soc Chem Ind*. 1939;58:1–7.
6. Kozeny J. Über kapillare Leitung des Wassers im Boden. *Sitzber Akad Wiss Wien*. 1927;136:270–306.
7. Stieß M. *Mechanische Verfahrenstechnik 2*. Berlin: Springer-Verlag, 1993.
8. Wakeman R, Tarleton S. *Solid Liquid Separation, Principles of Industrial Filtration*, 1st ed. Oxford: Elsevier, 2005.
9. Coulson JM, Richardson JF. *Chemical Engineering, Vol. 2: Unit Operations*, 3rd ed. Pergamon Press, *Chapter 4*.
10. Holdich R. *Fundamentals of Particle Technology*. Leicestershire: Midland Information Technology and Publishing, 2002.
11. Sorrentino JA, Anlauf H. Prediction of filter-cake properties from particle collective characteristics. *Fluid/Part Sep J*. 2004;16: 135–145.
12. Sorrentino JA. Advances in correlating filter cake properties with particle collective characteristics. PhD thesis, University of Karlsruhe. Germany: Shaker Verlag, 2002.
13. D'Arcy HPG. *Les fontaines publiques de la ville de Dijon: exosition et application des principles à suivre et des formules à employer dans les questions de distribution d'eau*. Paris: Victor Dalmont, 1856.
14. Beck R, Malthe-Sørenssen D, Andreassen J-P. Polycrystalline growth in precipitation of an aromatic amine derivative and L-Glutamic Acid. *J Cryst Growth*. 2009;311:320–326.
15. Beck R, Malthe-Sørenssen D, Andreassen J-P. The effect of crystallization conditions, crystal morphology and size on pressure filtration of L-glutamic acid and an aromatic amine. *Sep Purif Technol*. 2009;66:549–558.
16. Andreassen J-P. Formation mechanism and morphology in precipitaton of vaterite—nano-aggregation or crystal growth? *J Cryst Growth*. 2005;274:256–264.
17. Beck R, Andreassen J-P. The onset of spherulitic growth in crystallization of calcium carbonate. *J Cryst Growth*. 2010;312: 2226–2238.
18. Beck R, Andreassen J-P. Spherulitic growth of calcium carbonate. *Cryst Growth Des*. 2010;10:2934–2947.
19. Ogino T, Suzuki T, Sawada K. The formation and transformation mechanism of calcium carbonate in water. *Geochim Cosmochim Acta*. 1987;51:2757–2767.
20. Brečević L, Nielsen, AE. Solubility of amorphous calcium carbonate. *J Cryst Growth*. 1989;98:504–510.
21. Clarkson JR, Price TJ, Adams CJ. Role of metastable phases in the spontaneous precipitation of calcium carbonate. *J Chem Soc Faraday Trans*. 1992;88:243–249.
22. Plummer LN, Busenberg E. The solubilities of calcite, aragonite and vaterite in CO_2-H_2O solutions between 0 and 90°C, and an evaluation of the aqueous model for the system $CaCO_3$-CO_2-H_2O. *Geochim Cosmochim Acta*. 1982;46:1011–1040.
23. Andreassen J-P, Hounslow MJ. Growth and aggregation of vaterite in seeded-batch experiments. *AIChE J*. 2004;50:2772–2782.
24. Mullin JW. *Crystallization*, 4th ed. Oxford: Elsevier, 2001.
25. Kralj D, Brečević L, Nielsen AE. Vaterite growth and dissolution in aqueous solution I. Kinetics of crystal growth. *J Cryst Growth*. 1990;104:793–800.
26. Nývlt J, Ulrich J. *Admixtures in Crystallization*. Weinheim; New York; Basel; Cambridge; Tokyo: VCH, 1995.
27. Söhnel O, Garside J. *Precipitation: basic principles and industrial applications*. Oxford: Butterworth-Heinemann, 1992.
28. Braatz RD. Advanced control of crystallization processes. *Annu Rev Control*. 2002;26:87–99.

29. Müller M, Meier U, Wieckhusen D, Beck R, Pfeffer-Hennig S, Schneeberger R. Process development strategy to ascertain reproducible API polymorph manufacture. *Cryst Growth Des*. 2006;6: 946–954.
30. Liotta V, Sabesan V. Monitoring and feedback control of supersaturation using ATR-FTIR to produce an active pharmaceutical ingredient of a desired crystal size. *Org Process Res Dev*. 2004;8: 488–494.
31. Abu Bakar MR, Nagy ZK, Rielly CD. Seeded bach cooling crystallization with temperature cycling for the control of size uniformity and polymorphic purity of sulfathiazole crystals. *Org Process Res Dev*. 2009;13:1343–1356.
32. Abu Bakar MR, Nagy ZK, Saleemi AN, Rielly CD. The impact of direct nucleation control on crystal size distribution in pharmaceutical crystallization process. *Cryst Growth Des*. 2009;9: 1378–1384.
33. Aamir E, Nagy ZK, Rielly CD, Kleinert T, Judat B. Combined quadrature method of moments and method of characteristics approach for efficient solution of population balance models for dynamic modelling and crystal size distribution control of crystallization processes. *Ind Eng Chem Res*. 2009;48:8575–8584.
34. Nagy ZK. Model based robust control approach for batch crystallization product design *Comput Chem Eng*. 2009;33:1685–1691
35. Hounslow MJ, Reynolds GK. Product engineering for crystal size distribution. *AIChE J*. 2006;52:2507–2517.

Manuscript received June 3, 2010, revision received Nov. 21, 2010, and final revision received Jan. 13, 2011.